A novel model to predict phase equilibrium state of hydrates from the relationship of gas solubility

Jianbing Jiang[1], Jianxun Jiang[1]*, Jinchen Mao[1]*, Dong Li[2], Tuanhui Liu[3] and Zhong Pan[4]

[1]State Key Laboratory, Southwest Petroleum University, Chengdu, China, [2]Huabei Oilfield Third Oil Production Plant, PetroChina, Renqiu, China, [3]Gas Storage Branch of PetroChina Huabei Oilfield Company, Langfang, China, [4]Oil & Gas Technology Research Institute of Huabei Oilfield Company, Renqiu, China

The study of hydrate phase equilibrium is crucial for ensuring the safety of natural gas pipeline transportation and the process of hydrate recovery. While scientists typically focus on the chemical potential of hydrates, the role of gas solubility in hydrate phase equilibrium remains unclear, and this study fills this gap. This work investigated the solubility of gas at the equilibrium point of the hydrate phase through model calculations. Additionally, a new model of hydrate phase equilibrium is established based on the relationship between solubility. Firstly, a solubility model based on gas-liquid equilibrium theory showed higher prediction accuracy in comparison to the PR equation and Duan model and was then used to calculate gas solubility under hydrate phase equilibrium conditions. Afterwards, a novel model was developed to predict hydrate equilibrium state based on the relationship between gas solubility and hydrate phase equilibrium temperature, and it was further compared with the Chen−Guo model and CSMGem in terms of prediction accuracy under pure water and brine settings. The results showed: (a) The calculation deviation of the solubility model was 0.7−8.7% in pure water settings and 2.6−11.7% in brine settings; (b) A strong linear correlation between the phase equilibrium temperature of hydrates and gas solubility was also found; (c) This proposed model achieved over 10 times the accuracy of the Chen−Guo model and the CSMGem in predicting the phase equilibrium state of N_2 and CO_2 hydrates, and 3−10 times higher accuracy than that of the Chen−Guo model and CSMGem in brine. This work suggests that the gas solubility equilibrium theory can provide a more accurate prediction of hydrate states.

KEYWORDS

natural gas hydrate, gas solubility, prediction model, phase equilibrium, temperature, pressure

1 Introduction

Natural gas hydrates are a kind of non-stoichiometric crystalline structure substance and composed by gas and water molecules through hydrogen bonds. As a potential clean energy source, hydrate recovery has been gaining global attentions. Moreover, hydrates have the potential of applications in brine desalination (Sahu et al., 2018), storage (Cheng et al., 2020) and transportation of hydrogen (Lee et al., 2005; Strobel et al., 2009), CO_2 separation in flue gas, and CO_2 sequestration (Van Denderen et al., 2012; Quon and Jiang, 2023). In addition, hydrate plugs in pipeline for natural gas transportation are also a primary concern (Creek, 2012). Predicting hydrate deposition in natural gas pipelines is crucial for gas transportation efficiency and safety (Zhang et al., 2019a; Zhang et al., 2019b). The most common method to prevent the

hydrate-associated problems in the wellbore is to add a large amount of thermodynamic inhibitor to totally inhibit the formation of hydrates (hoon Sohn et al., 2015). Therefore, the evaluation of inhibitors also requires studying the phase equilibrium of hydrates. Moreover, accurate phase equilibrium analysis has a significant impact on the efficiency of gas exchange in natural gas hydrate recovery technology (Wang Y. et al., 2021), such as the equilibrium state of the hydrates can be broken by changing the temperature and pressure conditions of hydrate reservoirs (Qin et al., 2020). Temperature and pressure are the basic parameters for hydrate formation. Hydrate equilibrium state prediction is one of important aspects in the above hydrate-based technologies. Therefore, studying how to predict the temperature or pressure of hydrate phase equilibrium is significant.

The prediction methods for hydrate phase equilibrium mainly include the enthalpy–entropy chart method (Katz, 1945), thermodynamics model (Chen and Guo, 1996; Chen and Guo, 1998; Klauda and Sandler, 2000; Waals and Platteeuw, 2007), and neural network algorithm (Khamehchi et al., 2013; Xu et al., 2021). The enthalpy–entropy chart method is the earliest developed method, but it lacks an understanding of hydrate structures, leading to significant biases. The neural network method, including the application of multilayer perceptron and radial distribution function, have gradually become a hot research topic in recent years, but it exhibit overfitting (Khan et al., 2018). The thermodynamics models, including vdW-P type models (Waals and Platteeuw, 1958), Chen–Guo (C-G) model (Chen and Guo, 1996; Chen and Guo, 1998), and Klauda–Sandler (K-S) model (Klauda and Sandler, 2000), are well known and widely used. But these thermodynamics models rely on hypothesis (Wang L.-B. et al., 2021). The application range of the Antoine coefficient limits the applicability of the Chen Guo model (Mohammadi and Richon, 2008). Meanwhile, the main drawback of vdW-P model is its weak ability to predict high and low pressures and temperatures (Mohamadi-Baghmolaei et al., 2018). The original vdW-P model also exhibits a significant bias under high concentration salt solutions (Xu et al., 2021). Moreover, these models do not consider solubility and still require the calculation of gas fugacity or activity through equations of state (Li et al., 2019). On one hand, this is attributed to the low solubility of gases. On the other hand, these thermodynamic models construct the potential function of water molecules in hydrates, and it is independent of gas solubility. However, with the advancement of micro-molecular research in recent years, it has been gradually recognized that gas concentration plays a significant role in the influence of hydrates (Zhang et al., 2016; He et al., 2017).

The main factors affecting the phase equilibrium of hydrates include pressure (Liehui et al., 2006), salt (Lv et al., 2018), alcohol inhibitors (Sami et al., 2013), porosity (Yang et al., 2011), gas solubility and gas species. Experimental studies (Sloan and Koh, 2007) have found that the temperature of hydrate phase equilibrium is increased with increasing pressure. As the mineralization degree increases, the temperature of hydrate phase equilibrium decreases (Sloan and Koh, 2007). The higher the content of inhibitors, the lower the temperature of hydrate phase equilibrium (Sami et al., 2013). Additionally, the temperature of hydrates is varied for different natural gas species (Sloan and Koh, 2007). In recent years, some scholars have measured the solubility of greenhouse gases in the presence of hydrates (Li et al., 2018; Hassan et al., 2020; Wang et al., 2023). However, the relationship between gas solubility and the phase equilibrium temperature or pressure of natural gas hydrates is still unclear. It is difficult to observe or measure the gas saturate solubility

FIGURE 1
The workflow diagram for this work.
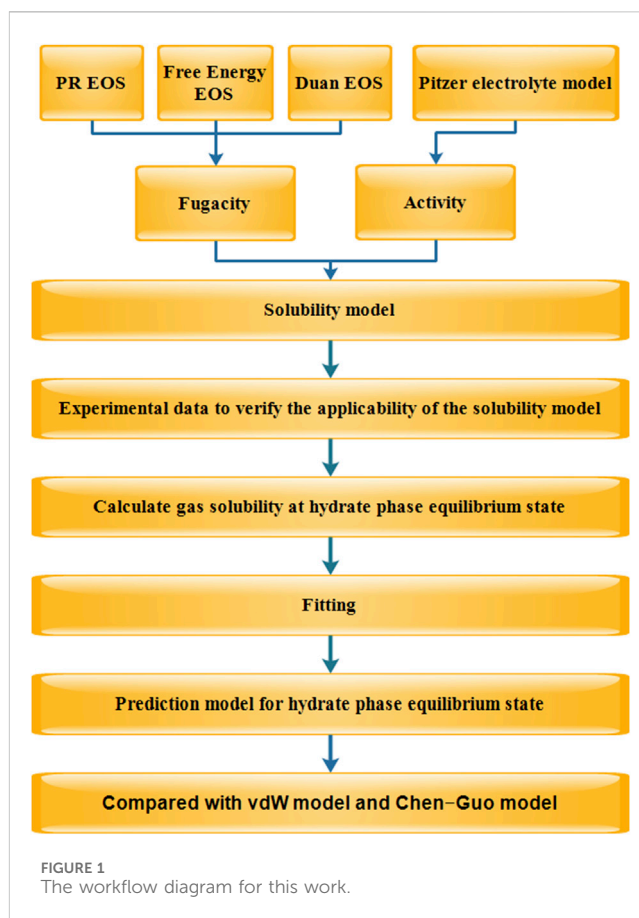
near hydrate formation in macroscopic experiments because the solubility exhibits supersaturation in the presence of hydrates (Song et al., 1997). Therefore, this work adopted high-precision solubility models for calculation. Studying the gas solubility before hydrate formation is of great significance for the investigation of hydrate phase equilibrium. It also holds reference significance for the study of hydrate nucleation concentration.

The main objective of this work is to study the solubility of gas in the vicinity of different hydrate equilibrium states. Subsequently, a model is constructed to predict the phase equilibrium of natural gas hydrates based on the relationship between gas solubility and the hydrate equilibrium state. Therefore, this study initially constructs a solubility model using gas-liquid theory to calculate the gas solubility at the hydrate equilibrium state. The solubility relationship is then fitted at various hydrate equilibrium temperatures. Furthermore, a novel model is developed based on gas solubility to predict the phase equilibrium state of natural gas hydrates. Finally, the Chen–Guo model and CSMGem software are compared with this model. Additionally, the equilibrium states of hydrates under pure water and brine conditions are predicted using this model.

2 Models description

The steps for this work can be broken down as follows:

(1) Constructing a gas solubility model suitable for high pressure based on gas-liquid phase equilibrium theory.

TABLE 1 Constants of Eqs 6–10.

C_i	CH_4[a]	CO_2[b]	N_2[c]	H_2S[d]	C_2H_6[e]	C_3H_8[e]
C1	8.3143711E+00	2.8944771E+01	−2.3093813E+01	4.2564957E01	−2.143686	0.513068
C2	−7.2772168E-04	−3.5458177E-02	5.6048525E-02	−8.6260377E-2	2.598765E-3	0.000958
C3	2.1489858E+03	−4.7706708E+03	9.8808898E+03	−6.0843775E3	4.6942351E2	
C4	−1.4019672E-05	1.0278277E-05	−5.1091621E-05	6.8714437E-5	−4.6849541E-5	
C5	−6.6743449E+05	3.3812610E+01	−1.3220298E+06	−1.0276849E2	−8.4616602E-10	
C6	7.6985890E-03	9.0403714E-03	−4.9542866E-04	8.4482895E-4	1.095219E-6	
C7	−5.0253331E-06	−1.1493403E-03	1.2698747E-06	−1.0590768		
C8	−3.0092013E+00	−3.0740573E-01	5.1411144E-01	3.5665902E-3		
C9	4.8468502E+02	−9.0730149E-02	−6.4733978E-05			
C10		9.3271134E-04				

[a](Duan and Mao, 2006).
[b](Duan and Sun, 2003).
[c](Mao and Duan, 2006).
[d](Duan et al., 2007).
[e](Li et al., 2015).

TABLE 2 Gas critical constant.

i	$T_{ci}(K)$	ρ_{ci} (mol/L)
CH_4	190.564	10.1393427
C_2H_6	305.322	6.8708545
C_3H_8	369.89	5.0000431
CO_2	304.1282	10.6249787
N_2	126.192	11.1839000
H_2S	373.37	10.19046

TABLE 3 Constants of Eq. 19.

m	i_m	j_m	k_m
1	1	1.5	0
2	1	0.25	0
3	1	1.25	0
4	3	0.250	0
5	7	0.875	0
6	2	1.375	0
7	1	0.00	1
8	1	2.375	1
9	2	2.000	1
10	5	2.125	1
11	1	3.5	2
12	1	6.5	2
13	4	4.75	2
14	2	12.5	3

(2) Calculating the gas solubility at hydrates phase equilibrium state

(3) Developing a predictive model for hydrate phase equilibrium state.

(4) Computing and comparing the reliability of the hydrate phase equilibrium state prediction model.

The workflow shows in Figure 1.

2.1 Gas-liquid equilibrium

The study of solubility can be broadly categorized into the fugacity-fugacity model and the fugacity-activity model. In the fugacity–activity model, gas equations of state (EOS), such as cubic equations (Soave, 1972; Peng and Robinson, 1976; Kontogeorgis et al., 2006) and multi parameter equations (Benedict et al., 1940; Benedict et al., 1951), are used to describe the gas phase, while electrolyte models are employed to describe aqueous solutions. It should be noted that cubic equations tend to exhibit increasing deviations under high-pressure conditions (Moshfeghian et al., 2012; Chabab et al., 2019; Rezania et al., 2021). Multiparameter equations are often preferred for high-pressure applications due to their higher accuracy. For instance, the Duan model (Duan et al., 1992) can be applied to pressures up to 2,000 bar for gases like CH_4 and CO_2. The SW96 (Span and Wagner, 1996) model (Span and Wagner, 1996) is capable of handling pressures up to 8,000 bar for CO_2 gas.

When the gas and liquid phases reach equilibrium, the chemical potential of component i in phases α and β can be expressed as follow:

$$\mu_i^{\alpha} = \mu_i^{\beta} \tag{1}$$

TABLE 4 Constants of a_m in Eq. 19.

m	a_m				
	CH$_4$	C$_2$H$_6$	C$_3$H$_8$	CO$_2$	N$_2$
1	1.8322924E+00	1.4106992E+00	8.9344622E-01	5.8478135E-01	1.8744499E+00
2	8.7789882E-01	9.5273464E-01	9.5710115E-01	9.5777220E-01	9.3065366E-01
3	−3.4460887E+00	−3.2800111E+00	−2.9259359E+0	−2.6415042E+00	−3.5352103E+00
4	6.2657087E-02	7.4487238E-02	8.1174579E-02	7.4935594E-02	6.4576333E-02
5	2.5615427E-04	2.7682993E-04	2.9457602E-04	2.1519215E-04	2.4160195E-04
6	−6.5955074E-02	−7.0645927E-02	−6.3671091E-02	−2.6666316E-02	−5.8692620E-02
7	−5.9610303E-02	−7.7537532E-02	−6.1187921E-02	1.3294773E-02	−6.0786818E-02
8	−3.1811362E-01	2.5014685E-02	2.5506442E-01	1.2546908E-01	−3.3794167E-01
9	−8.9264371E-02	2.2167878E-01	4.7835582E-01	4.2015287E-01	−1.3110278E-01
10	−2.0997734E-02	−1.5589363E-02	−8.4236341E-03	−1.2243601E-02	−2.5010756E-02
11	−5.9425962E-02	−2.2362512E-01	−3.2310881E-01	−2.5984348E-01	−2.1459359E-02
12	4.3560418E-03	−3.1480583E-04	3.1307119E-03	−1.7963087E-02	1.4669049E-03
13	1.9129741E-03	−4.7949598E-02	−7.7576991E-02	−6.1607536E-02	1.8683393E-02
14	1.7371647E-02	−1.7902771E-02	−2.5417583E-02	−1.9553446E-02	−1.7252238E-02

TABLE 5 Recommended values, where m (mol/kg) represents the mineralization degree of Na ions.

Component	C_i	D_i
CH$_4$	0.38532	0.001157634
C$_2$H$_6$	0.0689 + 0.012*m	0
C$_3$H$_8$	0.1701	0
CO$_2$	0.0708	0
N$_2$	0.0503	0
H$_2$S	0.0724	0

The chemical potential μ_i^V of the components in the vapor phase and chemical potential μ_i^l of the components in the liquid phase can be calculated as

$$\mu_i^V(T, P, y) = \mu_i^{V(\Theta)}(T) + RT \ln f_i(T, P, y)$$
$$= \mu_i^{V(\Theta)}(T) + RT\ln y_i P + RT \ln \varphi_i \quad (2)$$

$$\mu_i^l(T, P, m) = \mu_i^{l(\Theta)}(T, P) + RT \ln a_i(T, P, m_i)$$
$$= \mu_i^{l(\Theta)}(T, P) + RT \ln(N_w \times x_i) + RT \ln \gamma_i(T, P, m_i) \quad (3)$$

where i is the natural gas component, μ^V is the chemical potential gas component, μ^L is the chemical potential liquid component, a_i is the activity of component i, f_i is the fugacity of component i, φ_i is fugacity coefficient, γ_i is the activity coefficient, m_i is the solubility (in mol/kg water) of salt in the aqueous phase, N_w is the mole per kilogram of water (55.508 mol/kg), x_i is the mole fraction of species i in the liquid phase, $\mu_i^{V(\Theta)}$ is the standard chemical potential of species i in the non-aqueous phase, which is the ideal gas chemical potential at pressure of 1 bar, and

$\mu_i^{l(\Theta)}$ is the standard chemical potential of species i in an ideal aqueous solution with a hypothetical unit molality (Rowlinson, 1971). In the parameterization, the reference value $\mu_i^{V(\Theta)}$ can be set to 0 for convenience, because only the difference between $\mu_i^{V(\Theta)}$ and $\mu_i^{l(\Theta)}$ is important (Duan et al., 2007).

The equilibrium constant of component i can be defined as (Li and Duan, 2007):

$$\ln K_i = \frac{\mu_i^{V(\Theta)} - \mu_i^{l(\Theta)}}{RT} \quad (4)$$

Combining Eqs 1–4, we have:

$$y_i \varphi_i = N_w K_i x_i \gamma_i$$
$$m_i = x_i N_w = \frac{y_i \varphi_i}{K_i \gamma_i} \quad (5)$$

The functions for each component of natural gas are (Duan and Sun, 2003; Duan and Mao, 2006; Mao and Duan, 2006; Mao et al., 2013; Li et al., 2015)

$$\ln K_{CH_4}(T, P) = C_1 + C_2 T + \frac{C_3}{T} + \frac{C_4}{T^2} + \frac{C_5}{T^2} + C_6 P + C_7 PT + \frac{C_8 P}{T}$$
$$+ \frac{C_9 P}{T^2} + C_{10} P^2 T \quad (6)$$

$$K_{C_2H_6, C_3H_8}(T, P) = C_1 + C_2 T + \frac{C_3}{T} + C_4 T^2 + C_5 P + \frac{C_6 P}{T^2} + \frac{C_7}{P} \quad (7)$$

$$\ln K_{CO_2}(T, P) = C_1 + C_2 T + \frac{C_3}{T} + C_4 T^2 + \frac{C_5}{(630 - T)} + C_6 P$$
$$+ C_7 P \ln T + \frac{C_8 P}{T} + \frac{C_9 P}{(630 - T)} + \frac{C_{10} P^2}{(630 - T)^2}$$
$$+ C_{11} T \ln P \quad (8)$$

TABLE 6 Experimental data on the solubility of hydrocarbons in brine solutions and comparison.

Literature	Component	System	Temperature (K)	Pressure (bar)	N[a]	MH AAD (%)	Duan AAD (%)
Blount and Price (1982)	CH_4	Pure water	373.37–374.15	150–1,572	9	3.2	4.1
Price (1979)	CH_4	Pure water	444.3	400–1,600	6	5.7	5.9
Culberson and Mcketta (1951)	CH_4	Pure water	444.3	1.01–700	12	7.2	6.4
O'Sullivan and Smith (1970)	CH_4	Pure water	324.65	100–650	6	0.7	1.1
Addicks et al. (2002)	CH_4	Pure water	298.15	73.6–178.2	4	3.2	3.5
Kim et al. (2003)	CH_4	Pure water	298.15	23–166	6	4.2	4.3
Chapoy et al. (2004)	CH_4	Pure water	275.11–313.11	9.73–179.98	16	3.4	3.5
Wiebe and Gaddy (2002a)	CO_2	Pure water	323.15–373.15	23–703	19	2.3	2.7
Tödheide and Franck (1963)	CO_2	Pure water	323.15–533.15	200–2,000	20	7.2	6.1
Takenouchi and Kennedy (1964)	CO_2	Pure water	383.15–533.115	200–2,000	43	4.0	3.7
Addicks et al. (2002)	CO_2	Pure water	293.15	10.12–25.33	4	1.6	2.4
Fonseca et al. (2007)	CO_2	Pure water	290.27–302.93	1.01	14	1.2	1.9
Valtz et al. (2015)	CO_2	Pure water	298.28–318.23	4.65–79.63	34	3.3	4.1
Dalmolin et al. (2006)	CO_2	Pure water	293–323	0.98–4.6	35	3.8	3.4
Bermejo et al. (2005)	CO_2	Pure water	296.73–369.65	15.5–83.4	26	4.1	3.8
Koschel et al. (2006)	CO_2	Pure water	323.1	20–200	78	3.7	4.2
Chapoy et al. (2003)	N_2	Pure water	274–293	5–70	12	6.8	5.5
O'Sullivan and Smith (1970)	N_2	Pure water	398.15	100–620	6	3.0	3.5
Wiebe and Gaddy (2002b)	N_2	Pure water	323.15	20–1,012	8	1.9	2.2
Culberson and Mcketta (1951)	C_2H_6	Pure water	344.26–444.26	50–700	30	5.5	—
Mohammadi et al. (2004)	C_2H_6	Pure water	274.26–343.06	3.73–48.38	46	8.7	—
Kim et al. (2003)	C_2H_6	Pure water	298.15	14–39	9	7.0	—
Kobayashi and Katz (1953)	C_3H_8	Pure water	285.37–422.04	15–192	38	4.5	—
O'Sullivan and Smith (1970)	CH_4	0.056 m NaCl	374	100–1,550	9	2.6	3.1
Blount and Price (1982)	CH_4	0.91–5.7 m NaCl	324.65–512	100–1,550	37	3.8	3.6
Rumpf and Maurer (1994)	CO_2	4.0 m NaCl	353.1–433	8–100	16	6.3	6.5
Takenouchi and Kennedy (1964)	CO_2	1.09–4.28 m NaCl	423.15–523.15	100–1,400	50	8.8	4.9
Bermejo et al. (2005)	CO_2	0.249–0.10 m Na_2SO_4	298.4–345.02	19.8–127.9	106	5.8	4.7
Koschel et al. (2006)	CO_2	1.0–3.0 m NaCl	323.1; 373.1	20–200	11	3.5	2.9
O'Sullivan and Smith, (1970)	N_2	1.0–4.6 m NaCl	324.65, 375.65	100–610	22	2.5	1.6
Mishnina et al. (1961)	C_2H_6	1.0–6.0 m NaCl	288.15–348.15	1.01	28	11.7	—
Morrison and Billett (1952)	C_3H_8	0.5–6.0 m NaCl	285.74–344.85	1.01	28	9.5	—
Luis and Smith (1978)	CH_4	1.0 m $CaCl_2$	344.2	100–650	6	2.6	1.4
Stoessell and Byrne (1982)	CH_4	0.5–2.0 m $CaCl_2$	298.15–344.2	24–600	12	3.7	4.6
Prutton and Savage (1945)	CO_2	1.01–3.90 m $CaCl_2$	349.15–394.15	15–660	83	4.2	3.5
Byrne and Byrne (1982)	CH_4	0.0–4.0 m KCl	298.15	24.1–51.7	15	3.7	3.6

(Continued on following page)

TABLE 6 (*Continued*) Experimental data on the solubility of hydrocarbons in brine solutions and comparison.

Literature	Component	System	Temperature (K)	Pressure (bar)	N[a]	MH AAD (%)	Duan AAD (%)
Byrne and Byrne (1982)	CH_4	0.0–0.5 m K_2SO_4	298.15	24–52	9	7.6	8.4

[a]Number of data points; m represents mol/kg.

AAD is defined as $\sum_N \frac{1}{N} \frac{|V_{cal} - V_{exp}|}{V_{exp}}$, V_{cal} represents the model calculated data, and V_{exp} represents the experimental data. N is the number of experimental data.

$$\ln K_{N_2}(T, P) = C_1 + C_2 T + \frac{C_3}{T} + \frac{C_4}{T^2} + \frac{C_5}{T^2} + C_6 P + C_7 PT + \frac{C_8 P}{T} + \frac{C_9 P^2}{T^2} \tag{9}$$

$$\ln K_{H_2S}(T, P) = C_1 + C_2 T + \frac{C_3}{T} + C_4 T^2 + \frac{C_5}{(680 - T)} + C_6 P + \frac{C_7 P}{(680 - T)} + \frac{C_8 P^2}{T} \tag{10}$$

The constant c_i is shown in Table 1.

Consider the impact of water vapor, Consider the impact of water vapor, the calculation of gas composition is shown in Eqs (11, 12):

$$y_i = \frac{P - P_w^{sat}}{P} \tag{11}$$

P_w^{sat} is the saturated vapor pressure of water (Shibue, 2003):

$$\ln\left(\frac{P_w^{sat}}{P_c}\right) = \frac{1}{T_R}\left[\begin{array}{l} -7.85951783(1 - T_R) + 1.84408259(1 - T_R)^{1.5} - 11.7866497(1 - T_R)^3 \\ +22.6807411(1 - T_R)^{3.5} - 15.9618719(1 - T_R)^4 + 1.80122502(1 - T_R)^{7.5} \end{array}\right] \tag{12}$$

where $T_R = T/T_c$, T_c and P_c are the critical temperature and critical pressure, respectively, P_c = 22.064 MPa, T_c = 647.096 K.

2.2 Fugacity of nonaqueous species

In the multi-parameter equation of state, expressed in the form of Helmholtz free energy (MH), the free energy A is a function of temperature and density. It is expressed as the sum of the ideal state free energy and the remaining free energy (Mao et al., 2017), shows in Eqs (13–16):

$$A(\rho, T) = A^0(\rho, T) + A^r(\rho, T) \tag{13}$$

where ρ is density; A^0 is the ideal gas part of free energy; A^r is residual free energy.

The dimensionless Helmholtz free energy is defined as:

$$\alpha_i = \frac{A_i}{RT} \tag{14}$$

where A_i is pure component molar Helmholtz free energy;

$$\alpha_i = \alpha_i^0(\delta, \tau) + \alpha_i^r(\delta, \tau) \tag{15}$$

where δ and τ:

$$\begin{cases} \delta = \dfrac{\rho}{\rho_c} \\ \tau = \dfrac{T_c}{T} \end{cases} \tag{16}$$

where ρ_c and T_c is critical density and critical temperature, respectively, shows in Table 2.

The relationship between dimensionless Helmholtz Free Energy and PVT is shows in Eqs (17–19):

$$P = \rho RT\left[1 + \delta \alpha_{i\delta}^r(\delta, \tau)\right] \tag{17}$$

where

$$\alpha_{i\delta}^r = \frac{\partial \alpha^r}{\partial \delta} \tag{18}$$

$$\alpha_i^r(\delta, \tau) = \sum_{m=1}^{6} a_m \tau^{jm} \delta^{im} + \sum_{m=7}^{14} a_m \tau^{jm} \delta^{im} e^{-\delta^{k_m}} \tag{19}$$

The constants i, j, and k are shown in appendix Table 3, am is shown in Table 4.

The fugacity expression of the Mao's Helmholtz (MH) EOS (Mao et al., 2017) is shows in Eqs (20–22):

$$\ln \varphi_i = \left(\frac{\partial n a^r}{\partial n_i}\right)_{T,V,n_j} - \ln\left(1 + \delta a_\delta^r\right) \tag{20}$$

$$\left(\frac{\partial n a^r}{\partial n_i}\right)_{T,V,n_j} = a^r + n\left(\frac{\partial a^r}{\partial n_i}\right)_{T,V,n_j} \tag{21}$$

$$\begin{aligned} n\left(\frac{\partial a^r}{\partial n_i}\right)_{T,V,n_j} = \delta a_\delta^r\left[1 - \frac{1}{\rho_c}\left[\left(\frac{\partial \rho_c}{\partial x_i}\right)_{x_j} - \sum_{k=1}^{n} x_k\left(\frac{\partial \rho_c}{\partial x_k}\right)_{x_j}\right]\right] \\ + \tau a_\tau^r \frac{1}{T_C}\left[\left(\frac{\partial T_c}{\partial x_i}\right) - \sum_{k=1}^{n} x_k\left(\frac{\partial T_c}{\partial x_k}\right)_{x_j}\right] + a_{x_i}^r - \sum_{k=1}^{n} x_k a_{x_k}^r \end{aligned} \tag{22}$$

where α_δ^r, α_τ^r, and $\alpha_{x_i}^r$ are related derivatives of the residual free energy.
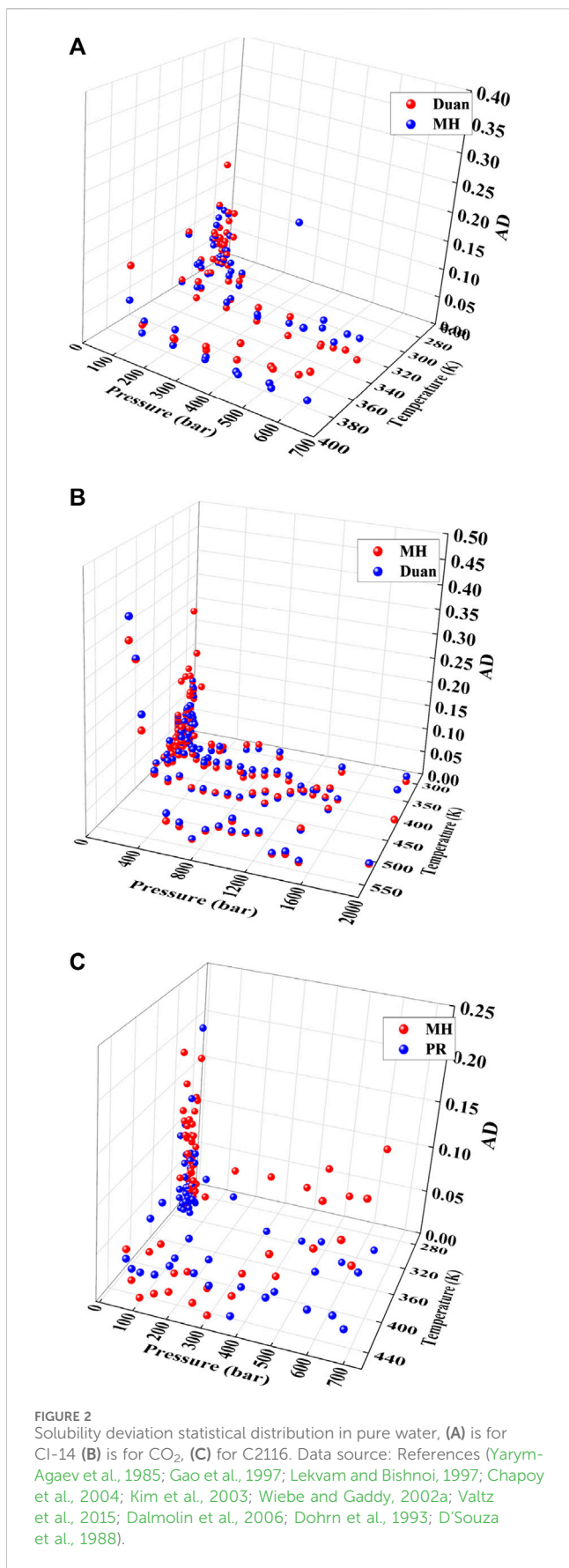
2.3 Activity coefficient model

The Pitzer activity coefficient model (Pitzer et al., 1984) can be expressed as

$$\ln \gamma_i = \sum_c 2\lambda_{i-c} m_c + \sum_a 2\lambda_{i-a} m_a + \sum_c \sum_a \xi_{i-c-a} m_c m_a \tag{23}$$

where m_c is the cation molality, mol/kg; m_a is the anion molality, mol/kg; λ_{i-c}, λ_{i-a} and ξ_{i-c-a} are coefficients that are a function of temperature and pressure and shows in Eqs 6–10, $\xi_{C_2H_6-Na^+-Cl^-} = -1.0165947 \times 10^{-2}$ and $\xi_{C_3H_8-Na^+-Cl^-} = -0.007485$.

For CH_4, CO_2, N_2, Eq. 5 can be transformed with Eq. 23 into Eqs (24–28):

$$\begin{aligned} \ln m_{CH_4} = {} & \ln\left(y_{CH_4} \varphi_{CH_4} P\right) - \ln K_{CH_4} \\ & - 2\lambda_{CH_4-Na^+}\left(m_{Na^+} + m_{K^+} + 2m_{Ca^{2+}} + 2m_{mg^{2+}}\right) \\ & - \xi_{CH_4-Na^+-Cl^-}\left(m_{Na^+} + m_{K^+} + 2m_{Ca^{2+}} + 2m_{mg^{2+}}\right) \\ & \times \left(m_{Cl^-} + 2m_{SO_4^{2-}}\right) - 4 \times 0.0332 m_{SO_4^{2-}} \end{aligned} \tag{24}$$

FIGURE 2
Solubility deviation statistical distribution in pure water, **(A)** is for CI-14 **(B)** is for CO_2, **(C)** for C2116. Data source: References (Yarym-Agaev et al., 1985; Gao et al., 1997; Lekvam and Bishnoi, 1997; Chapoy et al., 2004; Kim et al., 2003; Wiebe and Gaddy, 2002a; Valtz et al., 2015; Dalmolin et al., 2006; Dohrn et al., 1993; D'Souza et al., 1988).

$$
\begin{aligned}
\ln m_{CO_2} = {} & \ln\left(y_{CO_2}\varphi_{CO_2}P\right) - \ln K_{CO_2} \\
& - 2\lambda_{CO_2-Na^+}\left(m_{Na^+} + m_{K^+} + 2m_{Ca^{2+}} + 2m_{mg^{2+}}\right) \\
& - \xi_{CO_2-Na^+-Cl^-}\left(m_{Na^+} + m_{K^+} + 2m_{Ca^{2+}} + 2m_{mg^{2+}}\right)\left(m_{Cl^-}\right) \\
& + m_{SO_4^{2-}}\left(0.6593 log\left(P\right) - 1.5421/\log\left(T\right)\right)
\end{aligned}
\tag{25}
$$

$$
\begin{aligned}
\ln m_{N_2} = {} & \ln\left(y_{N_2}\varphi_{N_2}P\right) - \ln K_{N_2} \\
& - 2\lambda_{N_2-Na^+}\left(m_{Na^+} + m_{K^+} + 2m_{Ca^{2+}} + 2m_{mg^{2+}}\right) \\
& - \xi_{N_2-Na^+-Cl^-}\left(m_{Na^+} + m_{K^+} + 2m_{Ca^{2+}} + 2m_{mg^{2+}}\right) \\
& \times \left(m_{Cl^-} + 2m_{SO_4^{2-}}\right) + 4 \times 0.0371 m_{SO_4^{2-}}
\end{aligned}
\tag{26}
$$

$$
\begin{aligned}
\ln m_{C_2H_6} = {} & \ln\left(y_{C_2H_6}\varphi_{C_2H_6}P\right) - K_{C_2H_6} \\
& - 2\lambda_{C_2H_6-Na^+}\left(m_{Na^+} + m_{K^+} + 2m_{Ca^{2+}} + 2m_{mg^{2+}}\right) \\
& - \xi_{C_2H_6-Na^+-Cl^-}\left(m_{Na^+} + m_{K^+} + 2m_{Ca^{2+}} + 2m_{mg^{2+}}\right) \\
& \times \left(m_{Cl^-} + 2m_{SO_4^{2-}}\right)
\end{aligned}
\tag{27}
$$

$$
\begin{aligned}
\ln m_{C_3H_8} = {} & \ln\left(y_{C_3H_8}\varphi_{C_3H_8}P\right) - K_{C_3H_8} \\
& - 2\lambda_{C_3H_8-Na^+}\left(m_{Na^+} + m_{K^+} + 2m_{Ca^{2+}} + 2m_{mg^{2+}}\right) \\
& - \xi_{C_3H_8-Na^+-Cl^-}\left(m_{Na^+} + m_{K^+} + 2m_{Ca^{2+}} + 2m_{mg^{2+}}\right) \\
& \times \left(m_{Cl^-} + 2m_{SO_4^{2-}}\right)
\end{aligned}
\tag{28}
$$

2.4 Prediction model for hydrate phase equilibrium

The relationship between critical temperature of hydrate phase equilibrium and gas solubility can be given as follows:

$$
\frac{\partial \ln m_i}{\partial T} = C_i \; or \; \frac{\partial \ln m_i}{\partial T} = C_i + D_i T
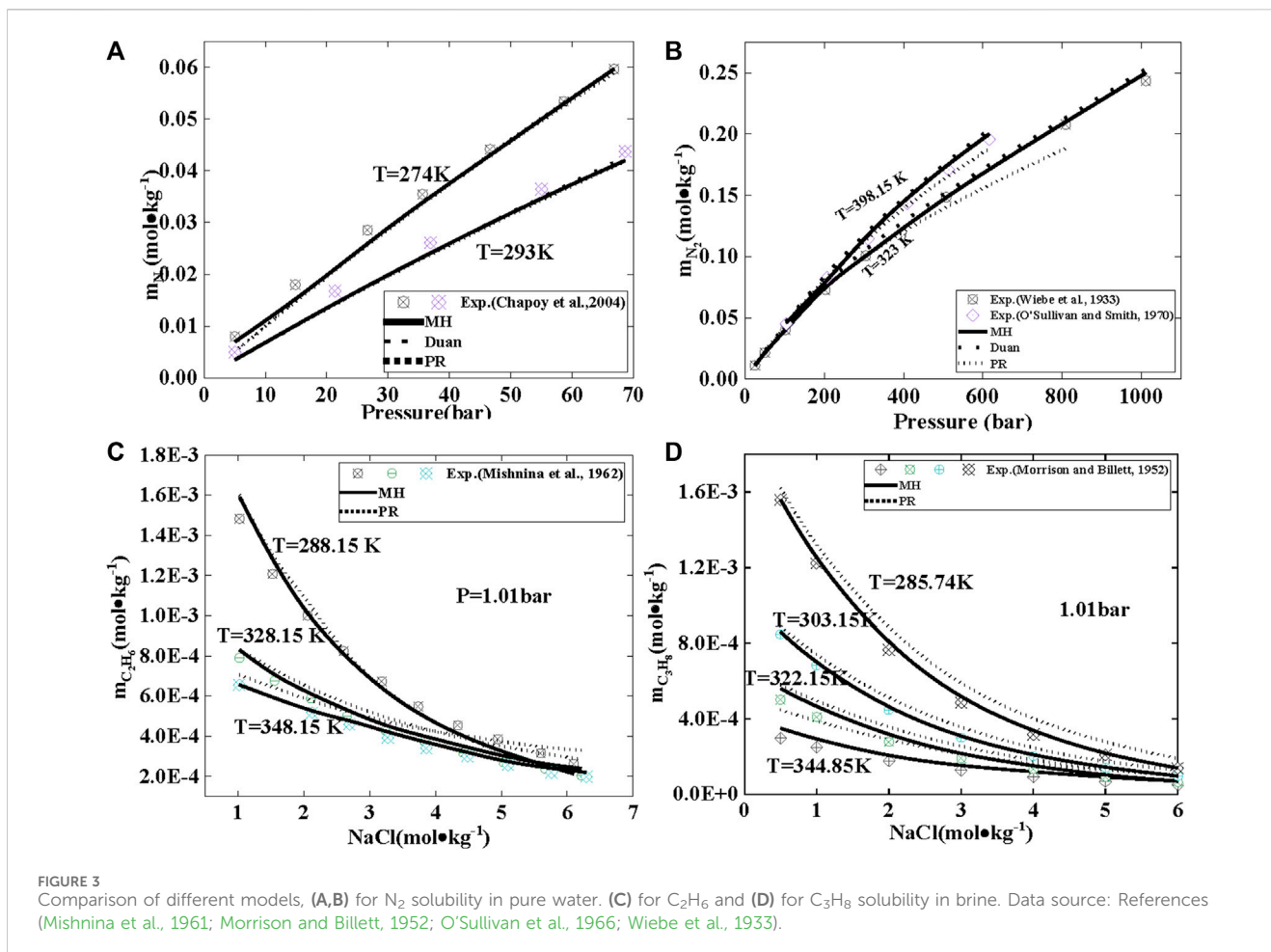\tag{29}
$$

Where i is component, m_i is gas solubility, C_i and D_i are constants, fitted by Origin 2021, shows in Table 5. This relationship will be demonstrated in the subsequent *Results* section. By combining Eqs 5, 29, a phase equilibrium prediction model for hydrate can be obtained:

$$
\frac{\partial \ln\left(\frac{y_i\varphi_i}{K_i\gamma_i}\right)}{\partial T} = C_i + D_i T
\tag{30}
$$

Eq. 30 can be transformed into:

$$
\frac{1}{\varphi_i}\frac{\partial \varphi_i}{\partial T} - \frac{1}{K_i\gamma_i}\frac{\partial \left(K_i\gamma_i\right)}{\partial T} = C_i + D_i T
\tag{31}
$$

The first term on the left-hand side of the equation is determined by EOS, while the second term is determined by the chemical potential of liquid. The constants C_i and D_i are determined by the composition of the system.

FIGURE 3
Comparison of different models, **(A,B)** for N_2 solubility in pure water. **(C)** for C_2H_6 and **(D)** for C_3H_8 solubility in brine. Data source: References
(Mishnina et al., 1961; Morrison and Billett, 1952; O'Sullivan et al., 1966; Wiebe et al., 1933).
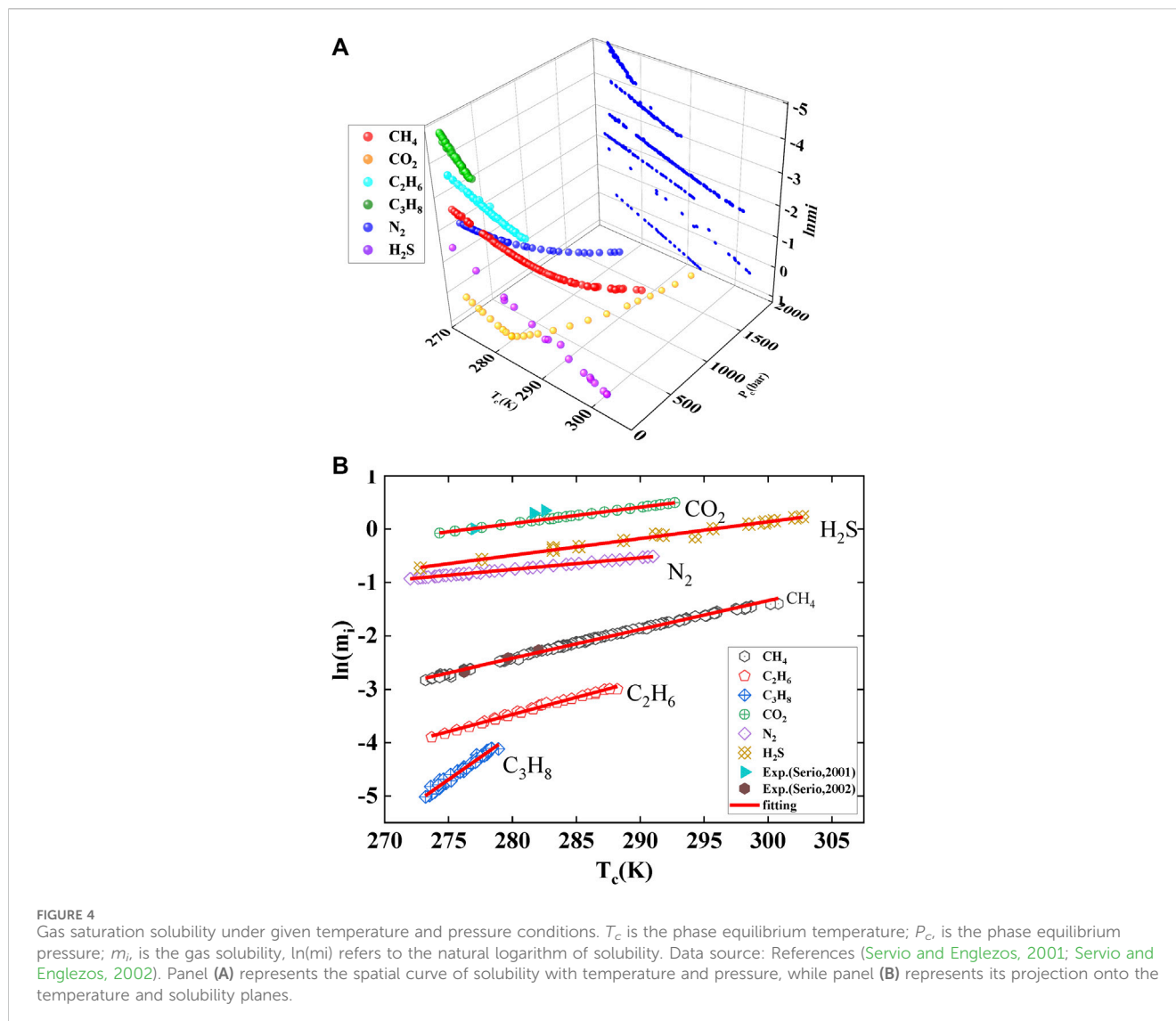
3 Results and discussion

3.1 Verification of the calculation accuracy of solubility

By comparing the experimental data with the solubility model, as shown in Table 6 solubility ranges from 0.7% to 7.6%, for CO_2 solubility ranges from 1.2% to 7.2%, and for N_2 solubility ranges from 1.9% to 6.8%. In comparison with Duan model, the MH model exhibits a deviation within 2%. Under low-temperature conditions, the solubility model shows good agreement with the experimental data, with an AAD of only 3.4%. The solubility of CH_4 and CO_2 under different conditions is analyzed, as depicted in Figures 2A, B, respectively. Apart from a small amount of experimental data deviating by approximately 10% under low-temperature (<280 K) and low-pressure (<100 bar) conditions for CH_4, most of the experimental data aligns with the calculated values of the model within a deviation of 5% or less. The prediction deviation of MH and Duan models for CO_2 generally remains within 5% under most data comparisons, with the peak deviation occurring under low–pressure and low–temperature conditions (288 K, 1.1 bar). Additionally, the model's deviation for CH_4 and CO_2 under high-pressure and low-temperature conditions is deemed acceptable.

The deviation of C_2H_6 solubility in the temperature range of 274 K–444 K and pressure range of 0bar–700 bar is statistically analyzed in Figure 2C. Within the pressure range less than 100 bar and temperature range of less than 280 K, the deviation between the MH model and experimental data is significant, with AD exceeding 10%. From Figure 2C, it can be seen that there is a significant deviation in some experimental data for the prediction results under low temperature and low-pressure conditions. This may be due to the low solubility of natural gas and the relative measurement deviation under low temperature and low-pressure conditions. Additionally, the presence of residual gases in water may also affect the results. Therefore, as the pressure increases and the solubility increases, this relative deviation would gradually decrease. When the pressure exceeds 100 bar, the deviation of the MH model becomes similar to that of the PR model, with AD around 5%. Therefore, under pure water conditions, the PR model is considered superior to the MH model.

The solubility for N_2 is shown in Figures 3A, B, the AADs of the MH, Duan, and PR models are 4.01%, 5.54%, and 4.51%, respectively. After pressure exceeds 500 bar (Figure 3B), the deviation of the PR (Peng-Robinson) model gradually increases. This is consistent with the results of literature research (Moshfeghian et al., 2012; Chabab et al., 2019). The PR equation has received widespread attention from scholars for its concise form,

FIGURE 4
Gas saturation solubility under given temperature and pressure conditions. T_c is the phase equilibrium temperature; P_c, is the phase equilibrium pressure; m_i, is the gas solubility, ln(mi) refers to the natural logarithm of solubility. Data source: References (Servio and Englezos, 2001; Servio and Englezos, 2002). Panel **(A)** represents the spatial curve of solubility with temperature and pressure, while panel **(B)** represents its projection onto the temperature and solubility planes.

but as the pressure gradually increases, the cubic equation of state shows an increasing bias. The advantage of the Duan model is that it accurately calculates the fugacity of pure gases, but the limitation of the Duan model is that it is only applicable to a limited number of pure gases.

The deviation of the model in calculating the solubility of gases under brine conditions is shown in Table 6, where the average absolute deviation (AAD) of the model for the solubility of CH_4, CO_2, and N_2 gases is acceptable. The distribution of calculation deviations for C_2H_6 solubility and C_3H_8 solubility using the MH model at different mineralization levels is shown in Figures 3C, D. The figure demonstrates that the MH model exhibits higher calculation accuracy compared to the PR model. The average absolute deviations (AAD) of the MH model for C_2H_6 and C_3H_8 are 11.7% and 9.5%, respectively. The model's calculation deviation is the smallest under low-temperature conditions (288.15 K for C_2H_6 and 285.74 K for C_3H_8) and increases with temperature. Furthermore, when the mineralization degree exceeds 4 mol/L, the deviation of the model in calculating the solubility of ethane increases. Therefore, the calculation deviation of the MH model is

considered acceptable for low temperatures and mineralization levels not exceeding 4 mol/L.

Through the verification of a large amount of experimental data, it can be observed that the gas solubility deviation of this solubility model under high-pressure conditions is primarily distributed within 10%, with some deviations even reaching 5%. This indicates that the calculated dissolution deviation near the hydrate phase equilibrium using this solubility model is acceptable. Although there is a significant deviation in the calculation of solubility under low-pressure and low-temperature conditions in this solubility model, it does not affect the usability of this solubility model since the formation conditions of natural gas hydrates occur under high pressure.

3.2 Relationship of solubility near hydrates

This work employs the MH model, Duan model, and PR model to calculate the gas solubility at the temperature and pressure of hydrate phase equilibrium. The pressure range considered in the
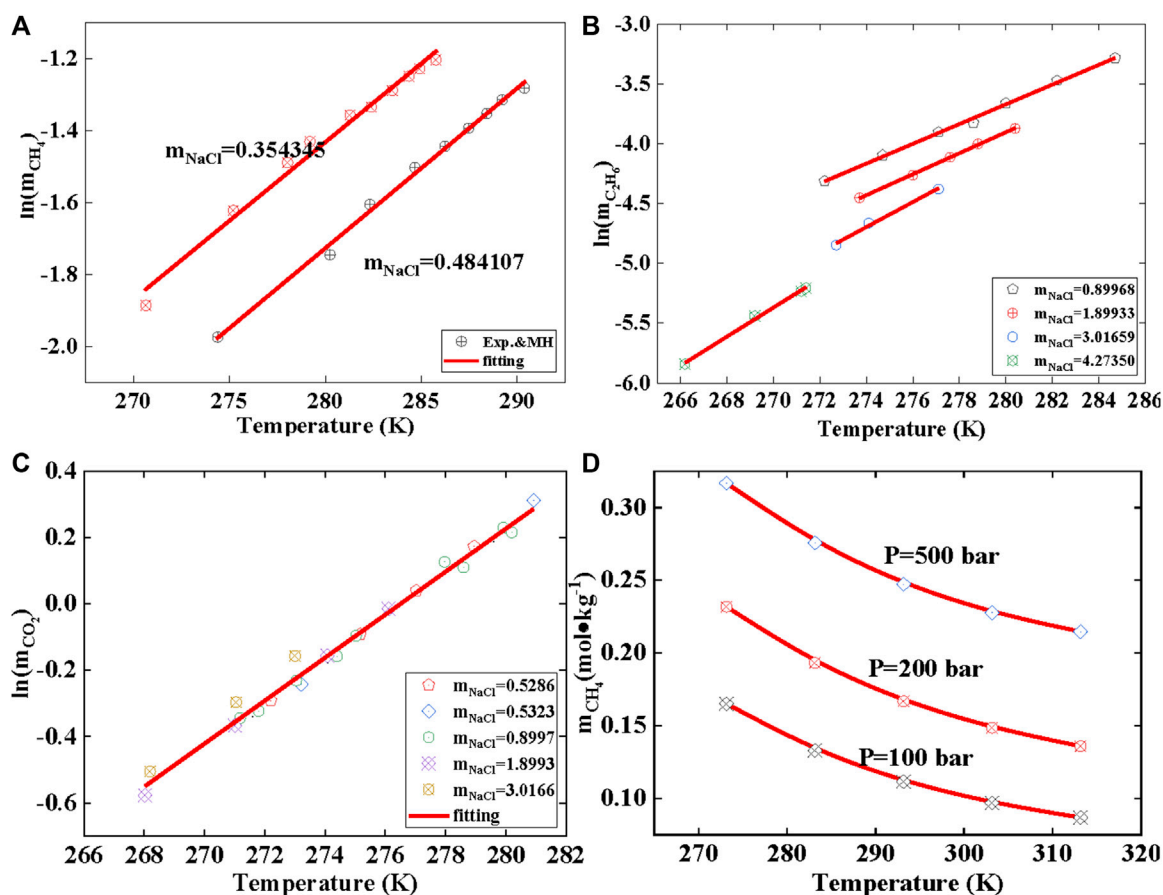
FIGURE 5
Solubility in brine condition and the gas solubility with temperature. Data source: References (Sloan and Koh, 2007). m represents solubility, mol/kg;
(A) represents the temperature-dependent solubility of methane at different mineralization levels; **(B)** represents the temperature-dependent solubility of ethane at different mineralization levels; **(C)** represents the temperature-dependent solubility of carbon dioxide at different mineralization levels, and **(D)** represents the temperature-dependent solubility of methane in pure water.

calculations is as follows: CH_4 (<2,000 bar), CO_2 (<2,000 bar), H_2S (<23 bar), N_2 (<1,000 bar), C_2H_6 (<33 bar), and C_3H_8 (<6 bar). The gas solubility at hydrate phase equilibrium is shown in Figure 4. All points in the figure represent three-phase equilibrium (gas-hydrate-liquid water), and the data points are obtained from the literature. The image in Figure 4A can be projected onto the solubility-temperature plane to obtain the linear graph shown in Figure 4B. The relationship between the natural logarithm of solubility and temperature follows a linear equation. Similarly, under brine conditions, the calculations yield a linear relationship, as shown in Figures 5A–C. Therefore, Eq. 29 can be easily derived. Normally, gas solubility decreases with increasing temperature, as depicted in Figure 5D. However, as the temperature of hydrate phase equilibrium increases, the gas solubility also increases, indicating a positive correlation between gas solubility and hydrate formation. Hence, gas solubility can be used to characterize the ease of hydrate formation. In other words, the higher the gas solubility, the higher the temperature at which the hydrate reaches phase equilibrium. This indicates that only a small temperature difference is required, but a significant pressure change is needed in the process of hydrate formation in two different states. However, the gas solubility required to produce hydrates in these two different states can be predicted linearly. In other words, obtaining hydrates at higher temperature conditions requires a higher gas solubility to be triggered.

In comparison to the experimental data provided by Servio (Servio and Englezos, 2001; Servio and Englezos, 2002), shows in Figure 4B, the experimental and calculated values for CH_4 show good agreement. However, there is a significant deviation between the calculated and experimental values for CO_2. This can be explained by the adsorption effect of hydrate (Song et al., 1997). This effect causes the aqueous solution to exhibit a supersaturation phenomenon.

3.3 Hydrate phase equilibrium prediction

3.3.1 Pure water setting

The prediction of methane hydrate phase equilibrium state is shown in Figure 6A; Table 7. As the pressure increases, the value predicted by this model is slightly lower than the experimental value, while the Chen–Guo model and CSMGem predict higher values. The curve of this model for CH_4 hydrate follows the trend of the experimental data more closely. This shows that the Chen–Guo model and vdWP thermodynamic models have a similar prediction
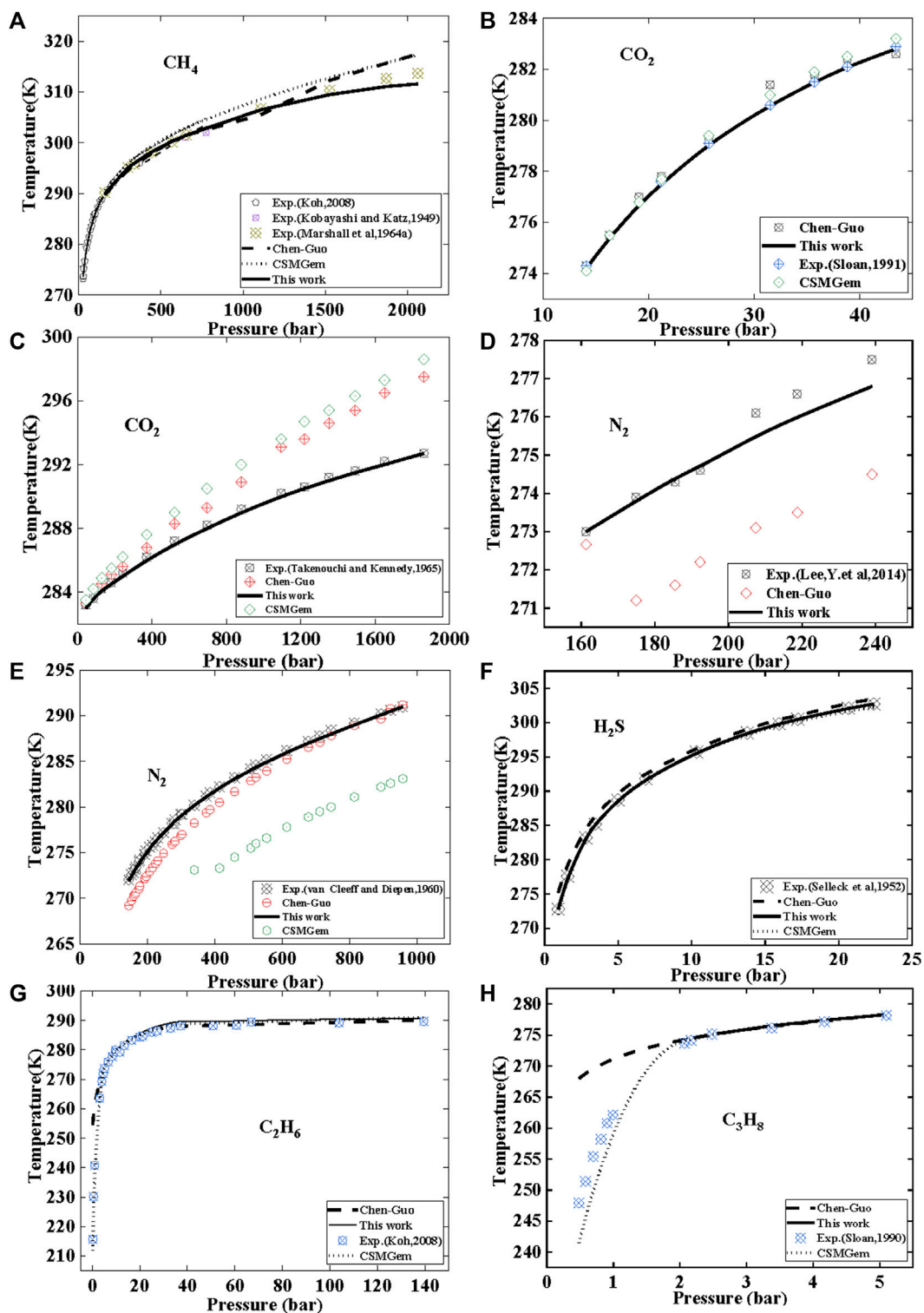
FIGURE 6
Comparison of this model with Chen—Guo model and CSMGem models for predicting the phase equilibrium of common gas hydrates.

accuracy for methane hydrates, but it is slightly lower than the prediction accuracy of this model.

For CO_2, the results compared with experimental data are shown in Figures 6B, C. At low-pressure conditions (Figure 6B),

the prediction accuracy of this model is similar to that of the Chen Guo model and CSMGem. However, under high–pressure conditions (Figure 6C), there is a significant difference in the prediction performance between this model and the Chen–Guo

TABLE 7 Comparison in pure water and brine setting. Data (Sloan and Koh, 2007).

Component	System	Pressure (bar)	Chen–Guo (AAD%)	CSMGem (AAD%)	This work (AAD%)
CH_4	water	0–2000	0.18	0.16	0.14
CO_2	water	10–20	0.09	0.07	0.02
CO_2	water	200–2000	0.65	0.9	0.05
N_2	water	160–200	0.89	NA	0.11
N_2	water	200–1,000	0.68	2.8	0.05
H_2S	water	0–25	0.3	0.07	0.01
C_2H_6	water	0–140	1.78	0.36	0.35
C_3H_8	water	0–5	0.09	0.078	0.01
CH_4	5–15wt%NaCl	0–800	0.28	0.24	0.33
CO_2	5–15wt%NaCl	10–45	1.6	1.9	0.12
C_2H_6	5–15wt%NaCl	0–30	0.47	0.19	0.14

model and CSMGem. This model demonstrates a better ability to predict CO_2 hydrate phase equilibrium state compared to the Chen–Guo model and CSMGem, with an AAD of only 0.02%–0.05%, while the Chen–Guo model has an AAD of 0.65%. The results of the Chen–Guo model are close to those of CSMGem, but the Chen–Guo model outperforms CSMGem for CO_2.

The prediction of N_2 hydrate phase equilibrium state was validated using experimental data, as shown in Figures 6D, E; Table 7. Under medium and low-pressure conditions (Figure 6D), the average absolute deviation (AAD) of this model is lower than that of the Chen-Guo model. Under high pressure (Figure 6E), CSMGem exhibited a significant deviation. Our model has an average absolute deviation (AAD) of 0.05%–0.11%, while the ChenGuo model and CSMGem have AADs of 0.68%–0.89% and 2.8%, respectively.

From Figures 6C–E, it can be seen that there is a significant difference in the prediction between this model and the thermodynamic models Chen Guo and vdWP(CSMGem). The prediction accuracy of this model can even be more than 10 times that of the latter two models. Firstly, this indicates that the model is more in line with experimental data. Secondly, this may be because the formation process of hydrates is a complex process, and thermodynamic models rely on numerous assumptions and empirical parameters. Finally, this also proves that the linear relationship between gas solubility and hydrate equilibrium temperature is worth studying in this article.

Comparing the predictions of the phase equilibrium state of H_2S hydrate using three models in Figure 6F; Table 7, the prediction deviation of this model is only 0.1%, while the prediction deviations of the Chen-Guo model and CSMGem software reach 0.3% and 0.07%, respectively. This indicates that this model has an advantage in terms of prediction accuracy.

The results of C_2H_6 hydrate are shown in Figure 6G; Table 7. It is observed that the AAD of this model is similar to that of CSMGem and better than that of the Chen–Guo model. The prediction results for C_3H_8 hydrate phase equilibrium state are presented in Figure 6H. The AAD of Chen–Guo mode is similar to
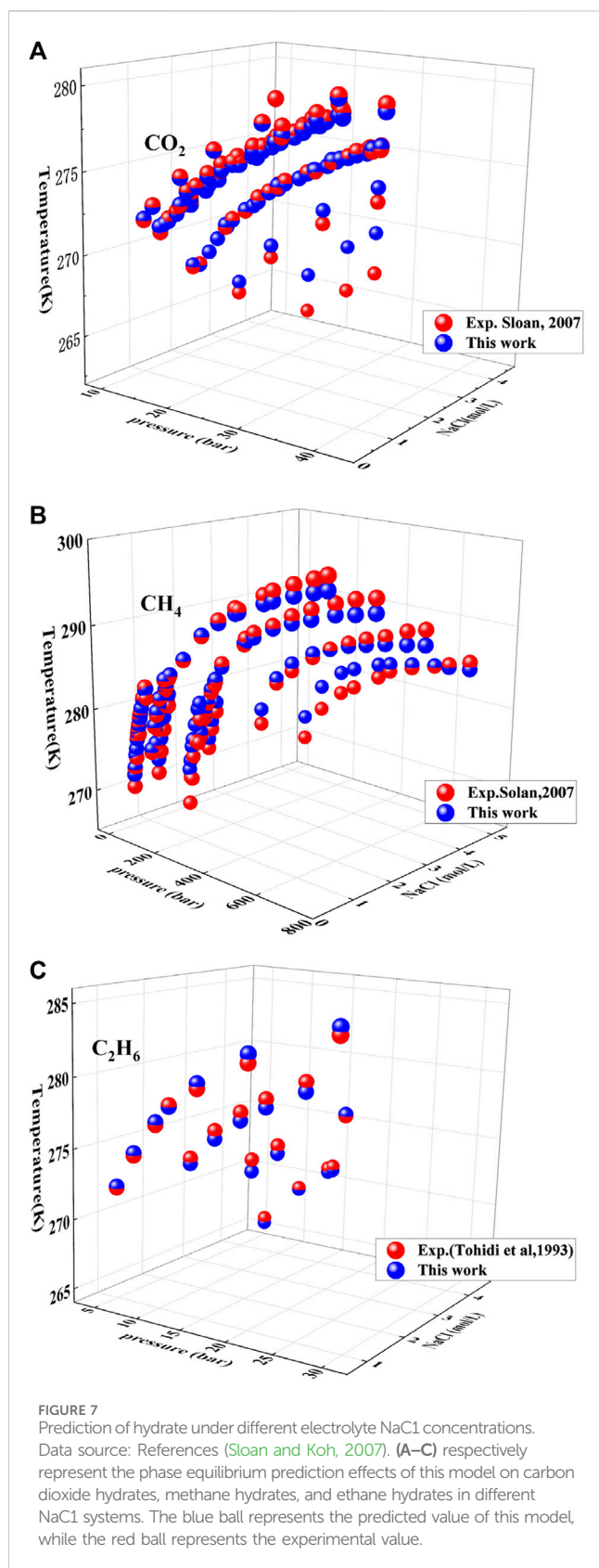
that of CSMGem and higher than that of this model. Similar to the Chen–Guo model, this model exhibits a significant deviation below 270 K, but its accuracy is nearly equivalent to that of the Chen–Guo model above 270 K. This deviation is caused by the conversion of the liquid phase to the ice phase when the temperature is below 273.15 K.

From Figure 6, it can be seen that this model has a significant advantage in predicting the equilibrium state of CO_2 and N_2 hydrates. The prediction accuracy for several hydrates such as CH_4, H_2S, C_2H_6, and C_3H_8 is similar to that of the thermodynamic models Chen–Guo and vdWP. As this model is derived based on GLE theory, it is only applicable to the equilibrium conditions of Liquid Water-Hydrate-Vapor. When the temperature is lower than 273 K, the system enters the ice-hydrate equilibrium phase. This model, along with the Chen–Guo model, shows a significant deviation in the ice-hydrate system. However, CSMGem exhibits a better prediction accuracy below the freezing point temperature.

3.3.2 Brine setting

The comparison of literature data between this model and the Chen–Guo model and CSMGem in brine is shown in Table 7. It shows that the accuracy of these three models is comparable in predicting CH_4 hydrate equilibrium. The AAD (average absolute deviation) of this model for predicting CO_2 and C_2H_6 hydrate equilibrium state is only 0.12%–0.33%, whereas the deviations of the Chen–Guo model and CSMGem reach 0.28%–1.6% and 0.19%–1.9%, respectively.

Under the presence of NaCl, the prediction for the CO_2 hydrate is shown in Figure 7A. The distance between the red and blue spheres represents the deviation between this model and the experimental data. The AAD of this model for CO_2 hydrate under electrolytes is 0.12%, but the deviation increases significantly when the temperature is below 270 K. As the salinity of electrolytes increases, it can be seen that the deviation progressively increases when the salinity of electrolytes over 4 mol/L. The deviation primarily arises from high concentrations of NaCl.

FIGURE 7
Prediction of hydrate under different electrolyte NaC1 concentrations. Data source: References (Sloan and Koh, 2007). **(A–C)** respectively represent the phase equilibrium prediction effects of this model on carbon dioxide hydrates, methane hydrates, and ethane hydrates in different NaC1 systems. The blue ball represents the predicted value of this model, while the red ball represents the experimental value.

The prediction of CH_4 hydrate formation under different NaCl concentrations is shown in Figure 7B, and the AAD of this model is 0.33%. Under low pressure (<200 bar) and low concentration NaCl conditions (<2 mol/L), the two sets of colored spheres almost overlap at

the same position, indicating that this model has high predictive accuracy for low temperature, low pressure, and low concentration conditions. The deviation of this model gradually increases with an increase in pressure. Additionally, as the concentration of NaCl increases, the deviation of the model's prediction also gradually increases. The figure demonstrates that electrolytes with concentrations greater than 4 mol/L have a significant impact on the prediction deviation of the model.

This model has a good prediction effect on hydrate under different NaCl mineralization degrees. The results are shown in Figure 7C, and it shows that the prediction results of this model are consistent with experimental data. Even if the NaCl mineralization degree reaches 4 mol/L, the deviation of the model is still small, and the AAD is 0.14%. Therefore, this model has strong prediction ability for C_2H_6 hydrate in low pressure condition.

In addition, this work also investigated and compared the improved Chen–Guo model and vdWP model, as shown in Table 8. The results show that compared to existing literature, this model has higher accuracy. The CPA, SRK, and PR equations are essentially cubic equations, and they generally exhibit a trend of increasing deviation under high-pressure conditions. Therefore, whether the cubic equation is coupled with the Chen Guo model or the vdWP model, it may exhibit a trend of increasing deviation under high pressure conditions.

From the above results, it is evident that as the mineralization degree increases, the prediction bias of the solubility model also increases, along with an increase in the calculation bias of the hydrate phase equilibrium state prediction model. This observation indicates that the predictive capability of the solubility model has a significant impact on the predictive ability of the hydrate phase equilibrium state model. Therefore, finding a high-precision solubility model for accurately predicting the phase equilibrium of hydrates holds great significance.

This model was used to predict hydrates under brine conditions, and a comparison was made between this model and two other models, namely, the Chen–Guo model and the vdWP model, to assess their calculation deviations. The results showed that this model exhibited higher accuracy compared to the other two models. On one hand, this demonstrates the reliability of the accuracy of this model. On the other hand, it indicates that there is still a strong linear relationship between gas solubility under brine conditions and the hydrate phase equilibrium temperature. As the salinity increases, the deviations of this model also gradually increase. This may be due to the fact that the calculation deviations of the solubility model also increase with increasing salinity. Additionally, it is known that salts act as hydrate inhibitors. Therefore, evaluating hydrate inhibitors could be a potential future application of this model.

4 Conclusion

This work investigates the relationship between the phase equilibrium state of hydrate and gas solubility. A prediction model for hydrate phase equilibrium state was constructed based on gas solubility. Firstly, a solubility model based on gas liquid equilibrium theory was constructed and compared with the PR equation and Duan model. The results showed that the MH can predict the gas solubility of CH_4, CO_2, and N_2 within the range of 0–2,000 bar. The deviation

TABLE 8 Comparison with existing literature models for predicting hydrate pressure.

Composition	System	Literature	Thermodynamic model description		This work (AAD%)
CH_4	water	El Meragawi et al. (2016)	PC-SAFT/vdWP	11.12	2.65
			PR/vdWP	6.86	
C_2H_6	water	El Meragawi et al. (2016)	PC-SAFT/vdWP	19.97	4.24
			PR/vdWP	20.05	
C_3H_8	water	El Meragawi et al. (2016)	PC-SAFT/vdWP	4.97	2.93
			PR/vdWP	4.9	
N_2	water	El Meragawi et al. (2016)	PC-SAFT/vdWP	2.64	0.85
			PR/vdWP	6.61	
CO_2	water	ZareNezhad and Ziaee (2013)	CPA/Chen–Guo	1.34	1.12
			SRK/vdW	3.12	
H_2S	water	ZareNezhad and Ziaee (2013)	CPA/Chen–Guo	3.17	0.71
			SRK/vdWP	6.26	

between the MH model and the Duan model is less than 2%. In the temperature range of 285–303 K and the NaCl concentration range of 0–6 mol/kg, the deviation of the MH model for CH_4, CO_2, and N_2 ranges from 0% to 5%. The deviation of the MH model for C_2H_6 solubility increases with higher temperature and mineralization. The MH model outperforms the PR model in calculating the solubility of C_2H_6 and C_3H_8 in brine, within the recommended range of salinity 0–4 mol/kg.

Furthermore, this study has found that as the temperature of the hydrates phase equilibrium increases, the gas solubility also increases. There is a strong linear relationship between the natural logarithm of gas solubility and the temperature of hydrate phase equilibrium. By utilizing this linear relationship, an empirical model for predicting the hydrate phase equilibrium state has been constructed. Comparing it to the classical Chen–Guo model and the vdW (CSMGem software) model, it was found that this model can achieve more than 10 times the accuracy of the Chen–Guo model in predicting the phase equilibrium of N_2 and CO_2 hydrates. Under the condition of 5–20wt% NaCl in brine, has an AAD of only 0.02%–0.05% and higher accuracy compare to the Chen–Guo model and CSGem software. This model is suitable for predicting hydrates of methane, ethane, propane, nitrogen, and hydrogen sulfide.

The proposed model in this work is based on gas solubility and applicable to conditions with Water-gas-hydrate system, such as natural gas pipelines. However, due to the lack of experimental data, the phase equilibrium of hydrates of C_3H_8, N_2, and H_2S under brine conditions was not predicted and compared in this work. This will be our focus in future work. In addition, this model may have potential applications in the evaluation of hydrate inhibitors.

Data availability statement

The original contributions presented in the study are included in the article/Supplementary material, further inquiries can be directed to the corresponding authors.

Author contributions

JbJ: Writing–original draft, Writing–review and editing, Software, Visualization. JxJ: Funding acquisition, Supervision, Writing–review and editing. JM: Supervision, Writing–review and editing. DL: Formal Analysis, Writing–review and editing. TL: Investigation, Validation, Writing–review and editing. ZP: Project administration, Writing–review and editing.

Funding

Conflict of interest

Author DL was employed by Huabei Oilfield Third Oil Production Plant, PetroChina. Author TL was employed by Gas Storage Branch of PetroChina Huabei Oilfield Company. Author ZP was employed by Oil and Gas Technology Research Institute of Huabei Oilfield Company.

The remaining authors declare that the research was conducted in the absence of any commercial or financial relationships that could be construed as a potential conflict of interest.

Publisher's note

All claims expressed in this article are solely those of the authors and do not necessarily represent those of their affiliated

References

Addicks, J., Owren, G. A., Fredheim, A. O., and Tangvik, K. (2002). Solubility of carbon dioxide and methane in aqueous methyldiethanolamine solutions. *J. Chem. Eng. Data* 47 (4), 855–860. doi:10.1021/je010292z

Benedict, M., Webb, G. B., and Rubin, L. C. (1940). An empirical equation for thermodynamic properties of light hydrocarbons and their mixtures I. Methane, ethane, propane and *n*-butane. *J. Chem. Phys.* 8 (4), 334–345. doi:10.1063/1.1750658

Benedict, M., Webb, G. B., and Rubin, L. C. (1951). An empirical equation for thermodynamic properties of light hydrocarbons and their mixtures I. Methane, ethane, propane and *n*-butane. *Fugacities liquid–vapour equilibria* 8 (4), 334–345. doi:10.1063/1.1750658

Bermejo, M. D., Martín, A., Florusse, L., Peters, C., and Cocero, M. (2005). The influence of Na_2SO_4 on the CO_2 solubility in water at high pressure. *Fluid Phase Equilibria* 238 (2), 220–228. doi:10.1016/j.fluid.2005.10.006

Blount, C. W., and Price, L. C. (1982). *Solubility of methane in water under natural conditions: a laboratory study.* United States: OSTI, 56–58.

Byrne, S., and Byrne, P. A. (1982). Salting-out of methane in single-salt solutions at 25°C and below 800 psia. *Geochimica Cosmochimica Acta* 46 (8), 1327–1332. doi:10.1016/0016-7037(82)90268-x

Chabab, S., Théveneau, P., Corvisier, J., Coquelet, C., Paricaud, P., Houriez, C., et al. (2019). Thermodynamic study of the CO_2-H_2O-NaCl system: measurements of CO_2 solubility and modeling of phase equilibria using Soreide and Whitson, electrolyte CPA and SIT models. *Int. J. Greenh. Gas Control* 91, 102825–102848. doi:10.1016/j.ijggc.2019.102825

Chapoy, A., Coquelet, C., and Richon, D. (2003). Solubility measurement and modeling of water in the gas phase of the methane/water binary system at temperatures from 283.08 to 318.12 K and pressures up to 34.5 MPa. *Fluid Phase Equilibria* 214 (1), 101–117. doi:10.1016/s0378-3812(03)00322-4

Chapoy, A., Mohammadi, A. H., Richon, D., and Tohidi, B. (2004). Gas solubility measurement and modeling for methane–water and methane–ethane–n-butane–water systems at low temperature conditions. *Fluid phase equilibria* 220 (1), 113–121. doi:10.1016/j.fluid.2004.02.010

Chen, G. J., and Guo, T. M. (1996). Thermodynamic modeling of hydrate formation based on new concepts. *Fluid Phase Equilibria* 122 (1-2), 43–65. doi:10.1016/0378-3812(96)03032-4

Chen, G.-J., and Guo, T.-M. (1998). A new approach to gas hydrate modelling. *Chem. Eng. J.* 71 (2), 145–151. doi:10.1016/s1385-8947(98)00126-0

Cheng, C., Wang, F., Tian, Y., Wu, X., Zheng, J., Zhang, J., et al. (2020). Review and prospects of hydrate cold storage technology. *Renew. Sustain. Energy Rev.* 117, 109492–109523. doi:10.1016/j.rser.2019.109492

Creek, J. (2012). Efficient hydrate plug prevention. *Energy and Fuels* 26 (7), 4112–4116. doi:10.1021/ef300280e

Culberson, O. L., and Mcketta, J. J. (1951). Phase equilibria in hydrocarbon-water systems III - the solubility of methane in water at pressures to 10,000 PSIA. *J. Petroleum Technol.* 3 (08), 223–226. doi:10.2118/951223-g

Dalmolin, I., Skovroinski, E., Biasi, A., Corazza, M., Dariva, C., and Oliveira, J. V. (2006). Solubility of carbon dioxide in binary and ternary mixtures with ethanol and water. *Fluid Phase Equilibria* 245 (2), 193–200. doi:10.1016/j.fluid.2006.04.017

Dohrn, R., Bünz, A. P., Devlieghere, F., and Thelen, D. (1993). Experimental measurements of phase equilibria for ternary and quaternary systems of glucose, water, CO_2 and ethanol with a novel apparatus. *Fluid Phase Equilibria* 83 (83), 149–158. doi:10.1016/0378-3812(93)87017-u

D'Souza, R., Patrick, J. R., and Teja, A. S. (1988). High pressure phase equilibria in the carbon dioxide -n-Hexadecane and carbon dioxide — water systems. *Can. J. Chem. Eng.* 66 (2), 319–323. doi:10.1002/cjce.5450660221

Duan, Z., and Mao, S. (2006). A thermodynamic model for calculating methane solubility, density and gas phase composition of methane-bearing aqueous fluids from 273 to 523 K and from 1 to 2000 bar. *Geochimica Cosmochimica Acta* 70 (13), 3369–3386. doi:10.1016/j.gca.2006.03.018

Duan, Z., and Sun, R. (2003). An improved model calculating CO_2 solubility in pure water and aqueous NaCl solutions from 273 to 533 K and from 0 to 2000 bar. *Chem. Geol.* 193 (3), 257–271. doi:10.1016/s0009-2541(02)00263-2

Duan, Z., Sun, R., Liu, R., and Zhu, C. (2007). Accurate thermodynamic model for the calculation of H_2S solubility in pure water and brines. *Energy and Fuels* 21 (4), 2056–2065. doi:10.1021/ef070040p

Duan, Z. H., Moller, N., and Weare, J. H. (1992). An equation of state for the CH4-CO2-H2O system: I. Pure systems from 0 to 1000°C and 0 to 8000 bar. *Academia* 56 (7), 2605–2617. doi:10.1016/0016-7037(92)90347-l

El Meragawi, S., Diamantonis, N. I., Tsimpanogiannis, I. N., and Economou, I. G. (2016). Hydrate–fluid phase equilibria modeling using PC-SAFT and Peng–Robinson equations of state. *Fluid Phase Equilibria* 413, 209–219. doi:10.1016/j.fluid.2015.12.003

Fonseca, I., Almeida, J., and Fachada, H. C. (2007). Automated apparatus for gas solubility measurements. *J. Chem. Thermodyn.* 39 (10), 1407–1411. doi:10.1016/j.jct.2007.05.013

Gao, J., Zheng, D. Q., and Guo, T. M. (1997). Solubilities of methane, nitrogen, carbon dioxide, and a natural gas mixture in aqueous sodium bicarbonate solutions under high pressure and elevated temperature. *J. Chem. Eng. Data* 42 (1), 69–73. doi:10.1021/je960275n

Hassan, M. H. A., Sher, F., Zarren, G., Suleiman, N., Tahir, A. A., and Snape, C. E. (2020). Kinetic and thermodynamic evaluation of effective combined promoters for CO2 hydrate formation. *J. Nat. Gas Sci. Eng.* 78, 103313. doi:10.1016/j.jngse.2020.103313

He, Z. J., Linga, P., and Jiang, J. W. (2017). *What are the key factors governing the nucleation of CO2 hydrate? Phys. Chem. Chem. Phys.* 19 (24), 15657–15661. doi:10.1039/c7cp01350g

hoon Sohn, Y., Kim, J., Shin, K., Chang, D., Seo, Y., Aman, Z. M., et al. (2015). Hydrate plug formation risk with varying watercut and inhibitor concentrations. *Chem. Eng. Sci.* 126, 711–718. doi:10.1016/j.ces.2015.01.016

Katz, D. L. (1945). Prediction of conditions for hydrate formation in natural gases. *Trans. AIME* 160 (01), 140–149. doi:10.2118/945140-g

Khamehchi, E., Shamohammadi, E., and Yousefi, S. H. (2013). Predicting the hydrate formation temperature by a new correlation and neural network. *Gas Process. J.* 1, 41–50. doi:10.22108/GPJ.2013.20158

Khan, M. N., Warrier, P., Peters, C. J., and Koh, C. A. (2018). Advancements in hydrate phase equilibria and modeling of gas hydrates systems. *Fluid Phase Equilibria* 463, 48–61. doi:10.1016/j.fluid.2018.01.014

Kim, Y., Ryu, S., Yang, S. O., and Lee, C. S. (2003). Liquid water–hydrate equilibrium measurements and unified predictions of hydrate-containing phase equilibria for methane, ethane, propane, and their mixtures. *Industrial Eng. Chem. Res.* 42 (11), 2409–2414. doi:10.1021/ie0209374

Klauda, J. B., and Sandler, S. I. (2000). A fugacity model for gas hydrate phase equilibria. *Industrial Eng. Chem. Res.* 39 (9), 3377–3386. doi:10.1021/ie000322b

Kobayashi, R., and Katz, D. (1953). Vapor-liquid equilibria for binary hydrocarbon-water systems. *Industrial Eng. Chem.* 45 (2), 440–446. doi:10.1021/ie50518a051

Kontogeorgis, G. M., Michelsen, M. L., Folas, G. K., Derawi, S., von Solms, N., and Stenby, E. H. (2006). Ten years with the CPA (Cubic-Plus-Association) equation of state. Part 1. Pure compounds and self-associating systems. *Industrial Eng. Chem. Res.* 45 (14), 4855–4868. doi:10.1021/ie051305v

Koschel, D., Coxam, J. Y., Rodier, L., and Majer, V. (2006). Enthalpy and solubility data of CO_2 in water and NaCl(aq) at conditions of interest for geological sequestration. *Fluid Phase Equilibria* 247 (1-2), 107–120. doi:10.1016/j.fluid.2006.06.006

Lee, H., Lee, J. W., Kim, D. Y., Park, J., Seo, Y. T., Zeng, H., et al. (2005). Tuning clathrate hydrates for hydrogen storage. *Nature* 434, 743–746. doi:10.1038/nature03457

Lekvam, K., and Bishnoi, P. R. (1997). Dissolution of methane in water at low temperatures and intermediate pressures. *Fluid Phase Equilibria* 131 (1), 297–309. doi:10.1016/s0378-3812(96)03229-3

Li, D., and Duan, Z. (2007). The speciation equilibrium coupling with phase equilibrium in the H_2O-CO_2-NaCl system from 0 to 250 °C, from 0 to 1000 bar, and from 0 to 5 molality of NaCl. *Chem. Geol.* 244 (3-4), 730–751. doi:10.1016/j.chemgeo.2007.07.023

Li, J., Zhang, Z., Luo, X., and Li, X. (2015). Modelling of phase equilibria in CH_4-C_2H_6-C_3H_8-nC_4H_{10}-NaCl-H_2O systems. *Appl. Geochem.* 56, 23–36. doi:10.1016/j.apgeochem.2015.02.006

Li, S., Li, Y., Yang, L., Chen, Y., Shao, Y., Sun, J., et al. (2019). Prediction of phase equilibrium of methane hydrate below 272.2 K based on different equations of state. *Fluid Phase Equilibria* 490, 61–67. doi:10.1016/j.fluid.2018.12.026

Li, Z., Wang, X., Xue, Q., and Liu, M. (2018). "Calculation for solubility of methane and carbon dioxide in water in presence of hydrate," in ISOPE International Ocean and Polar Engineering Conference, Sapporo, Japan, June 10–15, 2018.

Liehui, Z., Dengwei, L., and Yu, X. (2006). The experimental researches on phase equilibrium of natural gas hydrates. *Nat. Gas. Ind.* 26 (3), 129–130. doi:10.3321/j.issn: 1000-0976.2006.03.041

Luis, H., and Smith, N. O. (1978). The high pressure solubility of methane in aqueous calcium chloride and aqueous tetraethylammonium bromide. Partial molar properties of dissolved methane and nitrogen in relation to water structure. *J. Phys. Chem. B* 82 (2), 186–191. doi:10.1021/j100491a012

Lv, Q., Zang, X., Li, X., and Li, G. (2018). Effect of seawater ions on cyclopentane-methane hydrate phase equilibrium. *Fluid Phase Equilibria* 458, 272–277. doi:10.1016/j. fluid.2017.11.031

Mao, S., and Duan, Z. (2006). A thermodynamic model for calculating nitrogen solubility, gas phase composition and density of the N_2–H_2O–NaCl system. *Fluid Phase Equilibria* 248 (2), 103–114. doi:10.1016/j.fluid.2006.07.020

Mao, S., Lü, M., and Shi, Z. (2017). Prediction of the PVTx and VLE properties of natural gases with a general Helmholtz equation of state. Part I: application to the CH_4 -C_2H_6 -C_3H_8 -CO_2 -N_2 system. *Geochimica Cosmochimica Acta* 219, 74–95. doi:10. 1016/j.gca.2017.09.025

Mao, S., Zhang, D., Li, Y., and Liu, N. (2013). An improved model for calculating CO_2 solubility in aqueous NaCl solutions and the application to CO_2–H_2O–NaCl fluid inclusions. *Chem. Geol.* 347, 43–58. doi:10.1016/j.chemgeo.2013.03.010

Mishnina, T. A., Avdeeva, O. I., and Bozhovskaya, T. K. (1961). Solubility of gases in natural waters depending on temperature, pressure and salt composition. *Mater. Vses. Nauchn. Issled. Geol. Inst.* 46, 93–110. doi:10.1016/j.apgeochem.2015. 02.006

Mohamadi-Baghmolaei, M., Hajizadeh, A., Azin, R., and Izadpanah, A. A. (2018). Assessing thermodynamic models and introducing novel method for prediction of methane hydrate formation. *J. Petroleum Explor. Prod. Technol.* 8, 1401–1412. doi:10. 1007/s13202-017-0415-2

Mohammadi, A. H., Chapoy, A., Tohidi, B., and Richon, D. (2004). Measurements and thermodynamic modeling of vapor– liquid equilibria in ethane– water systems from 274.26 to 343.08 K. *Industrial Eng. Chem. Res.* 43 (17), 5418–5424. doi:10.1021/ie049747e

Mohammadi, A. H., and Richon, D. (2008). Thermodynamic model for predicting liquid water–hydrate equilibrium of the water–hydrocarbon system. *Industrial Eng. Chem. Res.* 47 (4), 1346–1350. doi:10.1021/ie0709640

Morrison, T. J., and Billett, F. (1952). 730. The salting-out of non-electrolytes. Part II. The effect of variation in non-electrolyte. *J. Chem. Soc.* 1952, 3819–3822. doi:10.1039/ jr9520003819

Moshfeghian, H. M., Azin, R., Hassanzadeh, H., and Moshfeghian, M. (2012). Mutual solubility of CH_4, CO_2, H_2S, and their mixtures in brine under subsurface disposal conditions. *Fluid Phase Equilibria* 324, 80–93. doi:10.1016/j.fluid.2012. 03.017

O'Sullivan, T. D., and Smith, N. O. (1970). Solubility and partial molar volume of nitrogen and methane in water and in aqueous sodium chloride from 50 to 125.deg. and 100 to 600 atm. *J. Phys. Chem.* 74 (7), 1460–1466. doi:10.1021/ j100702a012

O'Sullivan, T. D., smith, N. O., and Nagy, B. (1966). Solubility of natural gases in aqueous salt solutions—III nitrogen in aqueous NaCl at high pressures. *Geochimica Cosmochimica Acta* 30 (6), 617–619. doi:10.1016/0016-7037(66) 90015-9

Peng, D. Y., and Robinson, D. B. (1976). New two-constant equation of state. *Industrial Eng. Chem. Fundam.* 15 (1), 3069–3078. doi:10.1021/i160057a011

Pitzer, K. S., Peiper, J. C., and Busey, R. H. (1984). Thermodynamic properties of aqueous sodium chloride solutions. *J. Phys. Chem. Reference Data* 13 (1), 1–102. doi:10. 1063/1.555709

Price, L. C. (1979). Aqueous solubility of methane at elevated pressures and temperatures. *Aapg Bull.* 63 (9), 1527–1533. doi:10.1306/2F9185E0-16CE-11D7-8645000102C1865D

Prutton, C., and Savage, R. L. (1945). The solubility of carbon dioxide in calcium chloride-water solutions at 75, 100, 120° and high Pressures[1]. *J. Am. Chem. Soc.* 67 (9), 1550–1554. doi:10.1021/ja01225a047

Qin, X., Liang, Q., Ye, J., Yang, L., Qiu, H., Xie, W., et al. (2020). The response of temperature and pressure of hydrate reservoirs in the first gas hydrate production test in South China Sea. *Appl. Energy* 278, 115649. doi:10.1016/j.apenergy.2020. 115649

Quon, H., and Jiang, S. (2023). Decision making for implementing non-traditional water sources: a review of challenges and potential solutions. *npj Clean. Water* 6 (1), 56–14. doi:10.1038/s41545-023-00273-7

Rezania, P., Ranjbar, V., and Nasrifar, K. (2021). High pressure solubility of light gases (CH_4, C_2H_6, C_3H_8, H_2S, CO_2, N_2, Xe, Ar and Kr) and certain gas mixtures in water from cubic equations of state. *J. Solut. Chem.* 50, 1169–1188. doi:10.1007/s10953-021-01110-6

Rowlinson, J. S. (1971). *The principles of chemical equilibrium: kenneth denbigh.* 3rd Edn. Cambridge: University Press, 1195.

Rumpf, B., and Maurer, G. (1994). Solubility of ammonia in aqueous solutions of phosphoric acid: model development and application. *J. Solut. Chem.* 23 (1), 37–51. doi:10.1007/bf00972606

Sahu, P., Krishnaswamy, S., Ponnani, K., and Pande, N. K. (2018). A thermodynamic approach to selection of suitable hydrate formers for seawater desalination. *Desalination* 436, 144–151. doi:10.1016/j.desal.2018.02.001

Sami, N. A., Das, K., Sangwai, J. S., and Balasubramanian, N. (2013). *Phase equilibria of methane and carbon dioxide clathrate hydrates in the presence of (methanol+ MgCl₂) and (ethylene glycol+ MgCl₂) aqueous solutions. J. Chem. Thermodyn.* 65, 198–203. doi:10.1016/j.jct.2013.05.050

Servio, P., and Englezos, P. (2001). Effect of temperature and pressure on the solubility of carbon dioxide in water in the presence of gas hydrate. *Fluid phase equilibria* 190 (1-2), 127–134. doi:10.1016/s0378-3812(01)00598-2

Servio, P., and Englezos, P. (2002). Measurement of dissolved methane in water in equilibrium with its hydrate. *J. Chem. Eng. Data* 47 (1), 87–90. doi:10.1021/ je0102255

Shibue, Y. (2003). Vapor pressures of aqueous NaCl and $CaCl_2$ solutions at elevated temperatures. *Fluid Phase Equilibria* 213 (1-2), 39–51. doi:10.1016/s0378-3812(03)00284-x

Sloan, E. D., Jr, and Koh, C. A. (2007). *Clathrate hydrates of natural gases.* 3rd edition. United States: CRC Press, 360–500.

Soave, G. (1972). Equilibrium constants from a modified Redlich-Kwong equation of state. *Chem. Eng. Sci.* 27 (6), 1197–1203. doi:10.1016/0009-2509(72)80096-4

Song, K., Feneyrou, G., Fleyfel, F., Martin, R., Lievois, J., and Kobayashi, R. (1997). Solubility measurements of methane and ethane in water at and near hydrate conditions. *Fluid phase equilibria* 128 (1-2), 249–259. doi:10.1016/s0378-3812(96)03165-2

Span, R., and Wagner, W. (1996). A new equation of state for carbon dioxide covering the fluid region from the triple-Point temperature to 1100 K at pressures up to 800 MPa. *J. Phys. Chem. Ref. Data* 25 (6), 1509–1596. doi:10. 1063/1.555991

Stoessell, R. K., and Byrne, P. A. (1982). Salting-out of methane in single-salt solutions at 25°C and below 800 psia. *Geochimica Cosmochimica Acta* 46 (8), 1327–1332. doi:10. 1016/0016-7037(82)90268-x

Strobel, T. A., Hester, K. C., Koh, C. A., Sum, A. K., and Sloan, E. D. (2009). Properties of the clathrates of hydrogen and developments in their applicability for hydrogen storage. *Chem. Phys. Lett.* 478 (4-6), 97–109. doi:10.1016/j.cplett.2009. 07.030

Takenouchi, S., and Kennedy, G. C. (1964). The binary system H_2O+CO_2 at High temperatures and pressures. *Am. J. Sci.* 262 (9), 1055–1074. doi:10.2475/ajs.262.9. 1055

Tödheide, K., and Franck, E. U. (1963). Das zweiphasengebiet und die kritische kurve im system Kohlendioxid–Wasser bis zu drucken von 3500 bar. *Z. für Phys. Chem.* 37, 387–401. doi:10.1524/zpch.1963.37.5_6.387

Valtz, A., Chapoy, A., Coquelet, C., Paricaud, P., and Richon, D. (2015). Vapour–liquid equilibria in the carbon dioxide–water system, measurement and modelling from 278.2 to 318.2K. *Fluid Phase Equilibria* 226 (3), 333–344. doi:10. 1016/j.fluid.2004.10.013

Van Denderen, M., Ineke, E., and Golombok, M. (2012). CO_2 removal from contaminated natural gas mixtures by hydrate formation. *Industrial Eng. Chem. Res.* 48 (12), 5802–5807. doi:10.1021/ie8017065

Waals, J. H. v.d., and Platteeuw, J. C. (1958). Clathrate solutions. *Adv. Chem. Phys.* 2, 1–57. doi:10.1002/9780470143483.ch1

Waals, J. H. V. D., and Platteeuw, J. C. (2007). Clathrate solutions. *Adv. Chem. Phys.* 2, 1–57. doi:10.1002/9780470143483.ch1

Wang, L.-B., Cui, J.-L., Sun, C. Y., Ma, Q. L., Fan, S. S., Wang, X. H., et al. (2021b). Review on the applications and modifications of the Chen–Guo model for hydrate formation and dissociation. *Energy and Fuels* 35 (4), 2936–2964. doi:10.1021/acs. energyfuels.0c03977

Wang, X.-H., Xu, X.-J., Cai, J., Zheng, H. X., Chen, Y. X., Pang, W. X., et al. (2023). CO2 concentration in aqueous solution from gas–liquid equilibrium system to gas–liquid–hydrate coexistence system. *Gas Sci. Eng.* 115, 205024. doi:10.1016/j. jgsce.2023.205024

Wang, Y., Lang, X., Fan, S., Wang, S., Yu, C., and Li, G. (2021a). Review on enhanced technology of natural gas hydrate recovery by carbon dioxide replacement. *Energy and Fuels* 35 (11), 3659–3674. doi:10.1021/acs.energyfuels.0c04138

Wiebe, R., and Gaddy, V. L. (2002a). The solubility in liquid ammonia of hydrogen at 0° and of nitrogen at 0, 50, 75, 90 and 100° at pressures to 1000 atmospheres. Critical phenomena of ammonia-nitrogen Mixtures[1]. *J. Am. Chem. Soc.* 59 (10), 1984–1987. doi:10.1021/ja01289a055

Wiebe, R., Gaddy, V. L., and Heins, C., Jr. (1933). The solubility of nitrogen in water at 50, 75 and 100° from 25 to 1000 atmospheres. *J. Am. Chem. Soc.* 55 (3), 947–953. doi:10. 1021/ja01330a011

Wiebe, R., and Gaddy, V. L. (2002b). The solubility in water of carbon dioxide at 50, 75 and 100°, at pressures to 700 atmospheres. *J. Am. Chem. Soc.* 61 (2), 315–318. doi:10.1021/ja01871a025

Xu, H., Jiao, Z., Zhang, Z., Huffman, M., and Wang, Q. (2021). Prediction of methane hydrate formation conditions in salt water using machine learning algorithms. *Comput. Chem. Eng.* 151, 107358. doi:10.1016/j.compchemeng.2021.107358

Yang, M., Song, Y., and Liu, Y. (2011). Effects of porous media and salinity on phase equilibrium of methane hydrates. *J. Dalian Univ. Technol.* 51 (1), 31–35. doi:10.1007/s12182-011-0123-3

Yarym-Agaev, N. L., Sinyavskaya, R. P., and Koliushko, I. I. (1985). Phase equilibria in the water-methane and methanol-methane binary systems under high pressures. *J. Appl. Chem. USSR* 58 (1), 154–157.

ZareNezhad, B., and Ziaee, M. (2013). Accurate prediction of H_2S and CO_2 containing sour gas hydrates formation conditions considering hydrolytic and hydrogen bonding association effects. *Fluid Phase Equilibria* 356, 321–328. doi:10.1016/j.fluid.2013.07.055

Zhang, J., Wang, Z., Liu, S., Zhang, W., Yu, J., and Sun, B. (2019a). Prediction of hydrate deposition in pipelines to improve gas transportation efficiency and safety. *Appl. Energy* 253, 113521. doi:10.1016/j.apenergy.2019.113521

Zhang, J., Wang, Z., Sun, B., Sun, X., and Liao, Y. (2019b). An integrated prediction model of hydrate blockage formation in deep-water gas wells. *Int. J. Heat Mass Transf.* 140, 187–202. doi:10.1016/j.ijheatmasstransfer.2019.05.039

Zhang, Z. C., Liu, C. J., Walsh, M. R., and Guo, G. J. (2016). Effects of ensembles on methane hydrate nucleation kinetics. *Phys. Chem. Chem. Phys.* 18 (23), 15602–15608. doi:10.1039/c6cp02171a